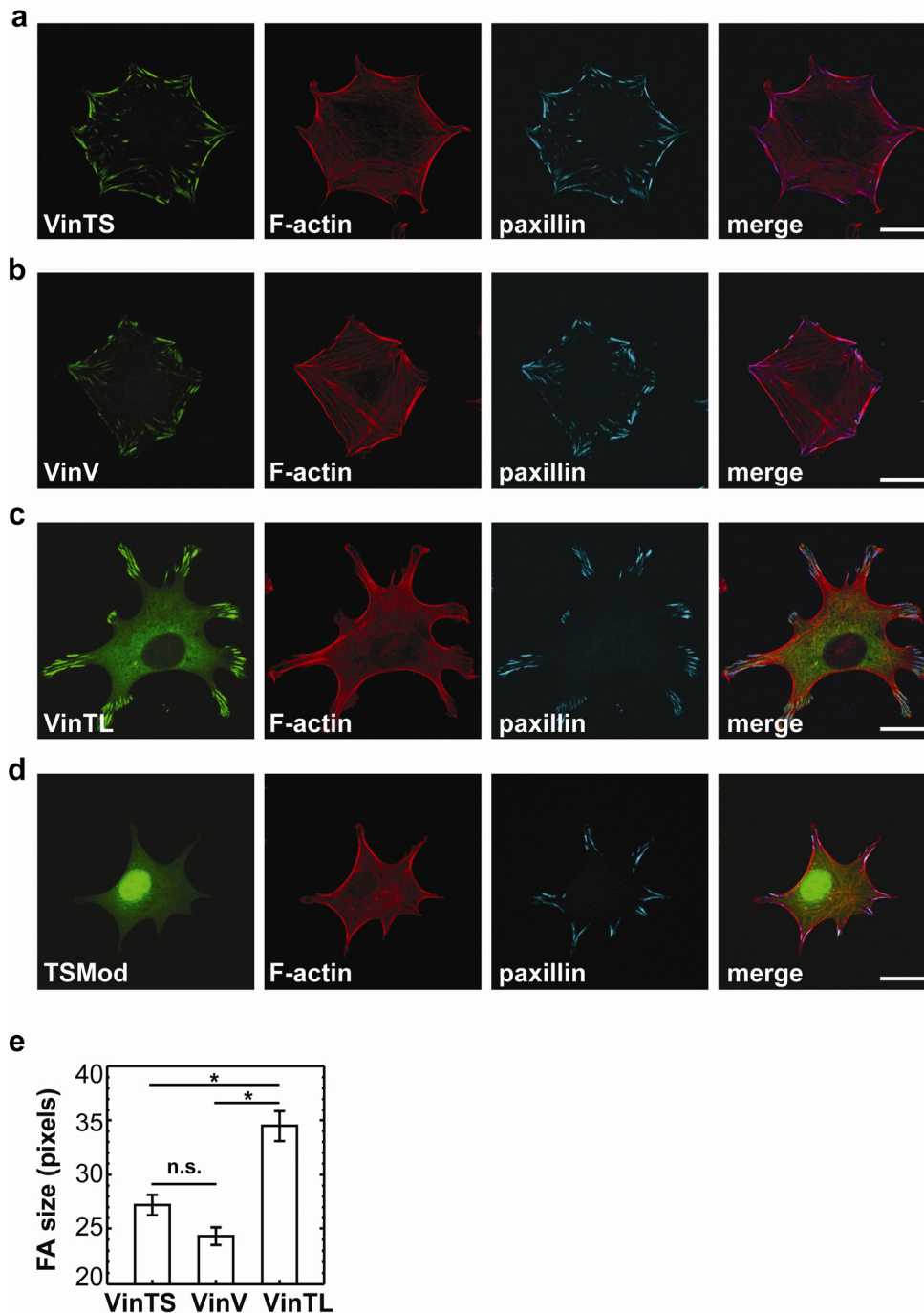
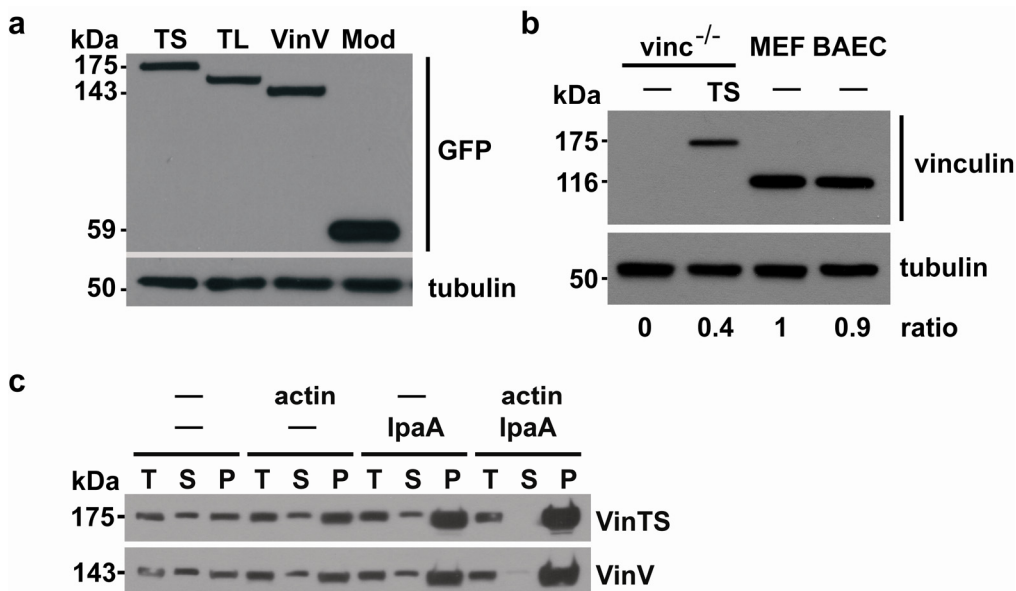


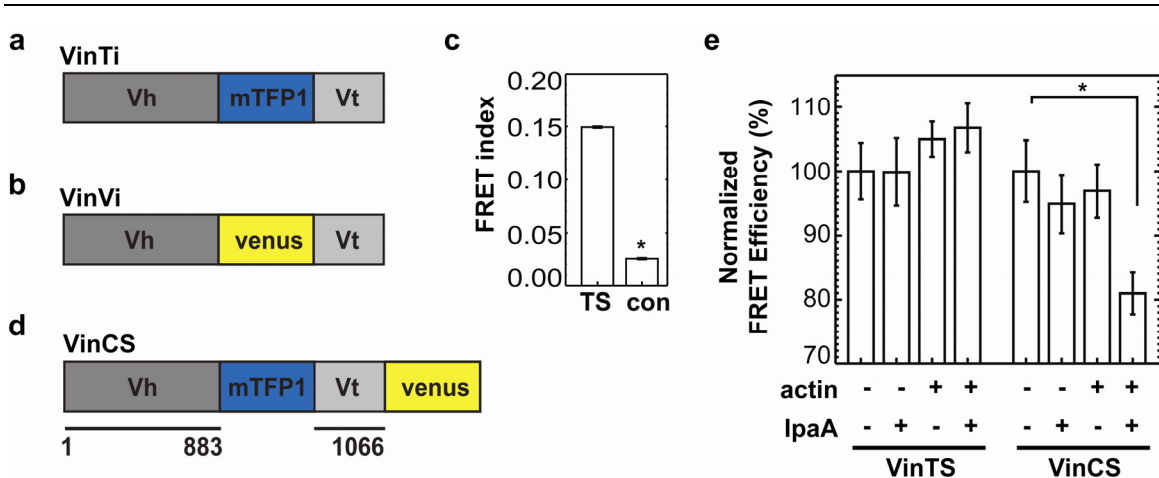
Supplementary Figures and Supplementary Figure Legends 1-9

Supplementary Fig.1. Localization of vinculin constructs. (a-d) Vinculin^{-/-} cells expressing VinTS (a), VinV (b), VinTL (c) or TSMMod (d) were stained for F-actin and paxillin. Scale bar: 20 μ m. (e) FA size quantification of VinTS, VinV and

VinTL expressed in vinculin^{-/-} cells. FAs of VinTL are significantly larger, while FAs of VinTS and VinV are not significantly different in size. (n=30 cells, *: p<0.0005, Tukey-b test). All error bars represent s.e.m.

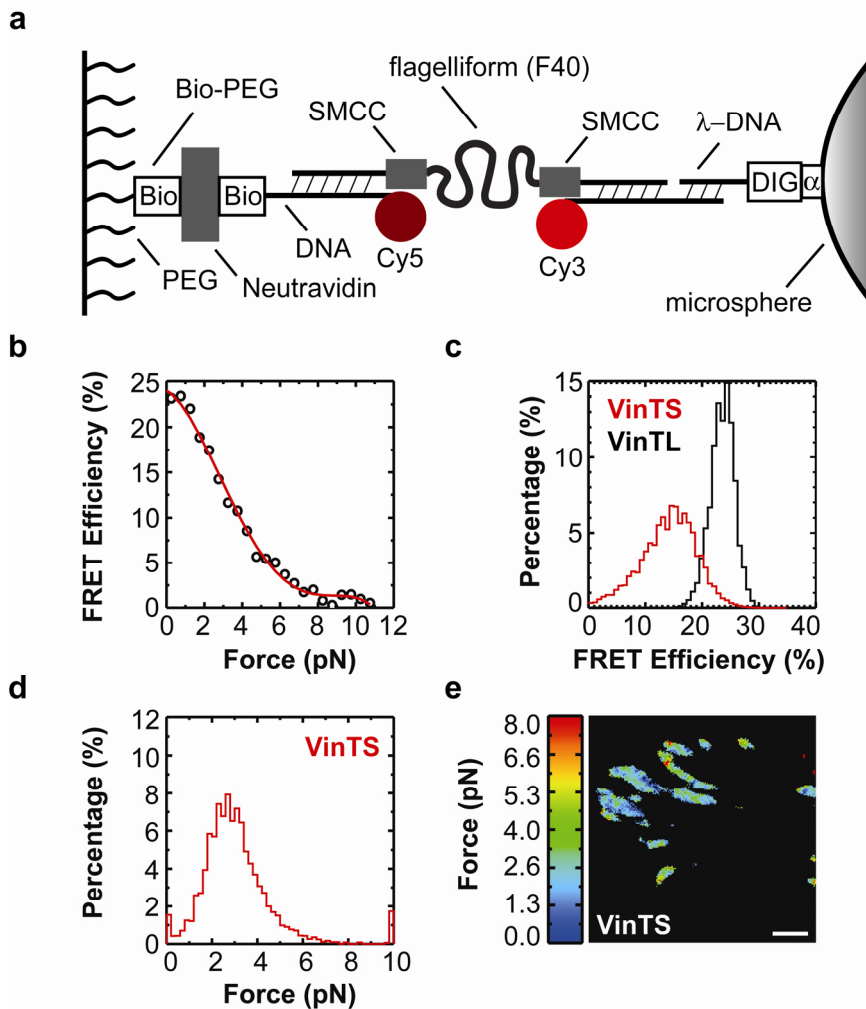


Supplementary Fig.2. Biochemical analysis of VinTS. (a) Western Blot of lysates from cells expressing VinTS, VinTL, VinV or TSMod. (b) Expression levels of transiently transfected vinculin^{-/-} cells (transfection efficiency: ~43 %) were compared to endogenous vinculin in MEFs and BAECs. (c) Vinculin sedimentation assay using hypotonic lysates of HEK293 cells expressing VinTS or VinV. (T: total, S: supernatant; P: pellet). Equal amounts of protein from each fraction were subjected to SDS-PAGE and Western blotting; these represent 4 % of the fraction for T and S, and 50 % for P.



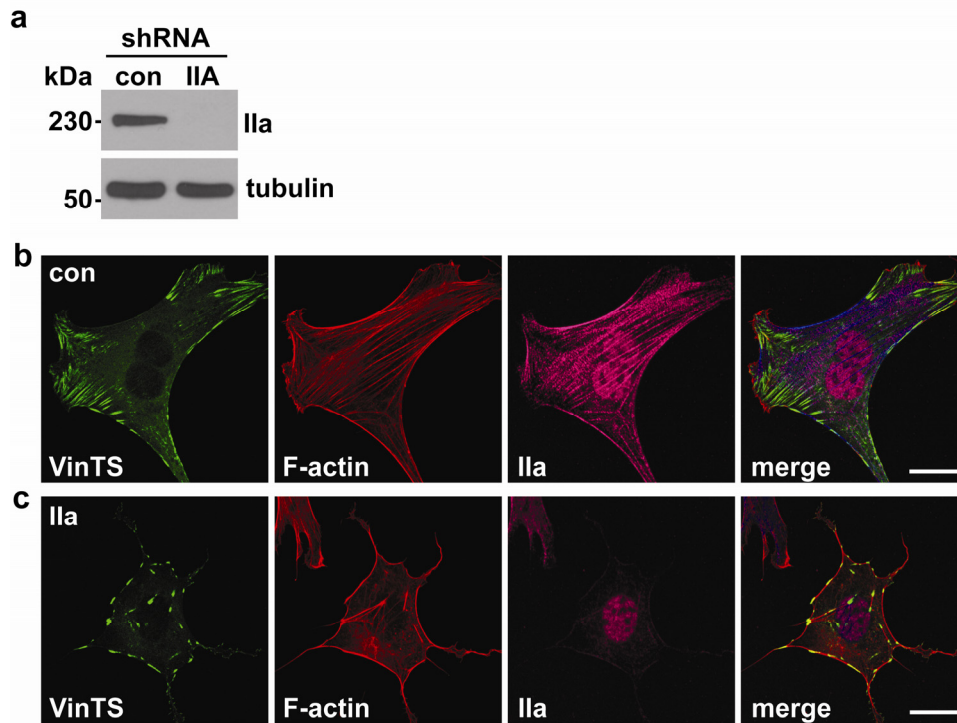
Supplementary Fig.3. Conformation and inter-molecular FRET controls. (a)

Vinculin with internal mTFP1 (VinTi). (b) Vinculin with internal venusA206K (VinVi). (c) FRET index of vinculin^{-/-} cells expressing VinTS, or both VinTi and VinVi (con). (n=20, *: p<0.00001). (d) The vinculin conformation sensor (VinCS) contains an internal mTFP1 after aa 883 and a C-terminal venusA206K. (e) FRET was determined by spectrofluorimetry of hypotonic lysates from cells expressing VinTS and VinCS in the presence or absence of 2 μ M IpaA and 5 μ M actin (n=4, *: p=0.03, Dunnet's test). All error bars represent s.e.m.

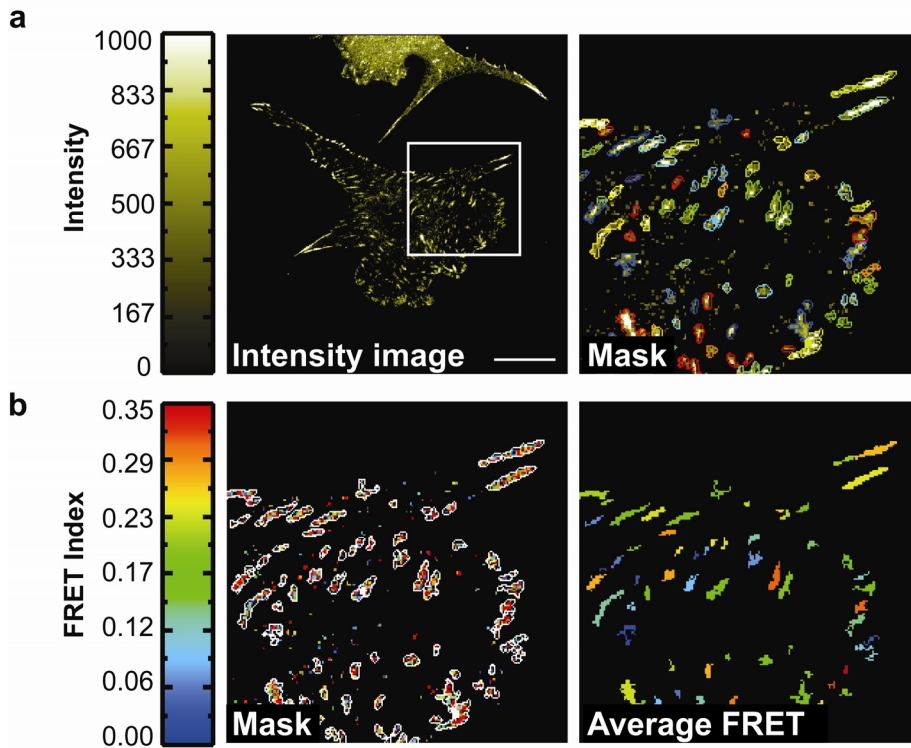


Supplementary Fig.4. Single molecule experiments and force calculations.

(a) Experimental setup of single molecule force-FRET measurements of TSMOD. Bio: biotin, DIG: digoxigenin, PEG: polyethylenglycol, Bio-PEG: biotinylated-PEG, α : anti-digoxigenin. (b) FRET efficiency-force estimation of TSMOD. The red line is a fourth order polynomial fit utilized for numerical conversions. (c) FRET efficiency histograms from FAs of VinTS ($n=11$) or VinTL ($n=8$) expressing vinculin^{-/-} cells. (d) Lifetime histogram of VinTS shown in (Fig.2d) was converted using (b) to display the force distribution across VinTS in FAs of vinculin^{-/-} cells. (e) Lifetime image of VinTS shown in (Fig.2c) was converted using (b) to determine the average force/molecule. Scale bar: 2 μ m.

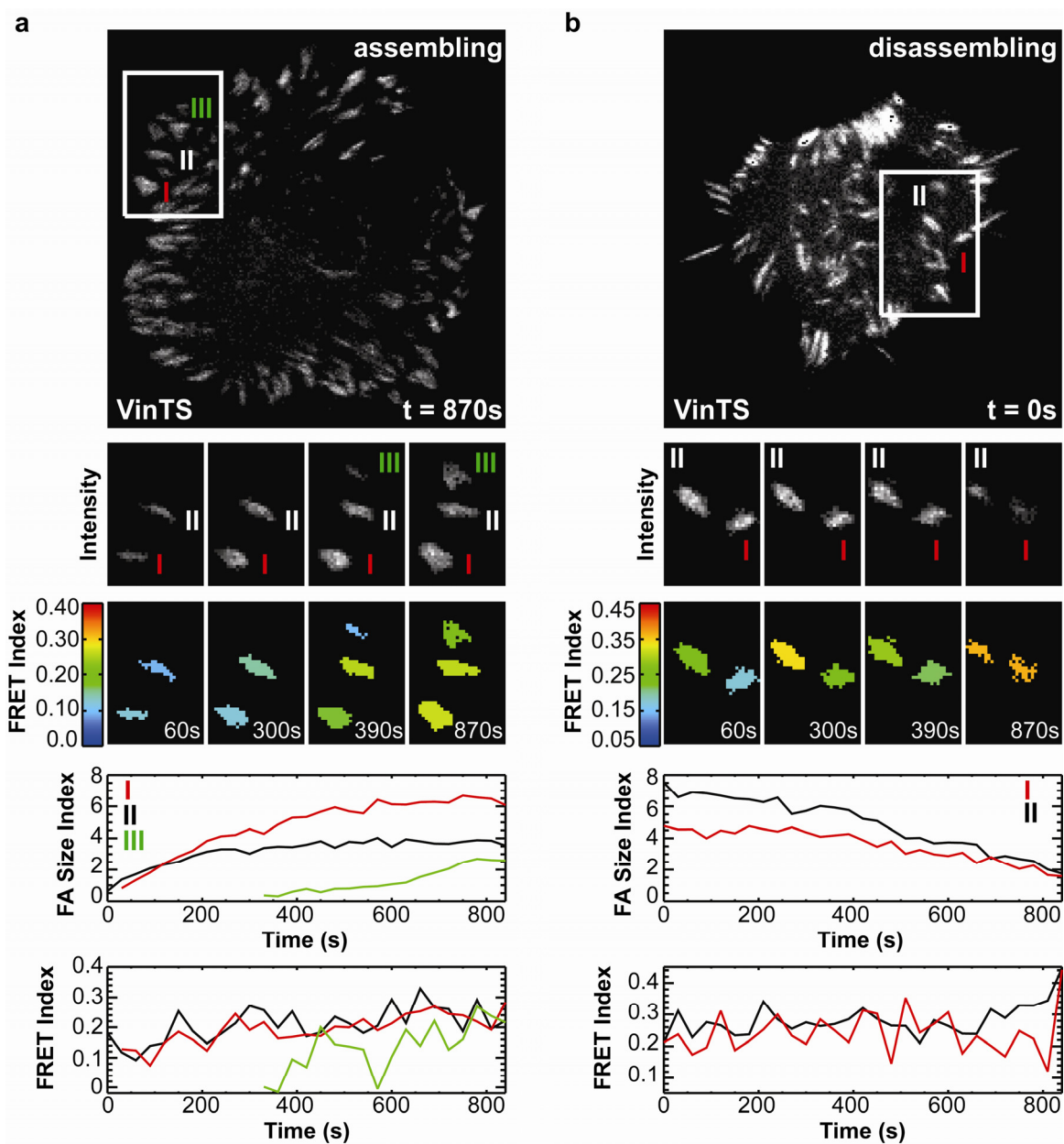


Supplementary Fig.5. Depletion of myosin Ila in vinculin^{-/-} cells. (a) Western Blot analysis of lysates from vinculin^{-/-} cells expressing pSUPER-control (con) or the previously described pSUPER-MIIa (IIa)³¹. (b, c) Vinculin^{-/-} cells expressing VinTS and pSUPER-control, or VinTS and pSUPER-MIIa were immunostained for myosin Ila and F-actin. Scale bar: 20 μ m.



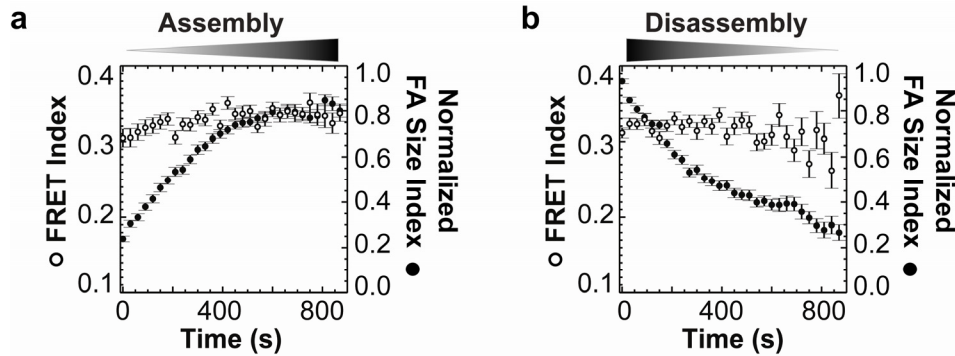
Supplementary Fig.6. FA isolation (water algorithm) and FA FRET analysis.

(a) The water algorithm was run on the intensity image from the venusA206K channel to isolate single FAs and to define FA masks shown in (b). (c) Masks were applied to the FRET index images and other channels (not shown). (d) FRET index within individual FA mask was averaged to enhance statistical power.

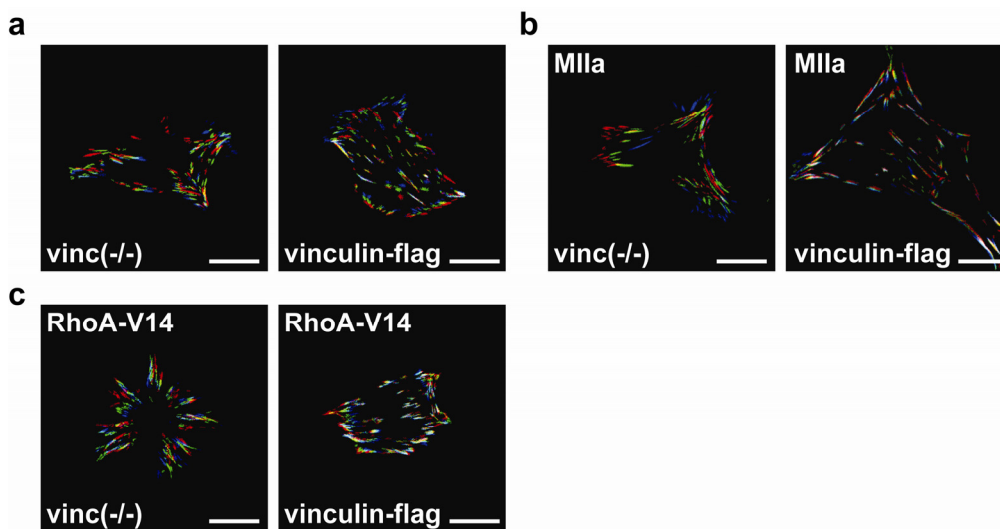


Supplementary Fig.7. FRET in assembling and disassembling FAs. (a, b)

The water algorithm was combined with particle tracking software to identify assembling (a) or disassembling (b) FAs. (a) FRET index in small assembling FAs is low and increases as FAs grow. (b) Disassembling FAs display high FRET index which further increases as FAs shrink. FA Size Index is the size of the FA (in pixels) multiplied by its average intensity.



Supplementary Fig.8. VinTL FRET during FA assembly / disassembly. FAs in VinTL expressing cells were isolated, tracked and classified as assembling ($n=100$) or disassembling ($n=104$). (a, b) No change in FRET index was observed. All error bars represent s.e.m.



Supplementary Fig 9. EGFP-paxillin dynamics with or without vinculin. (a-c) Cells expressing EGFP-paxillin were analyzed by time-lapse imaging. FA movement was emphasized by assigning a different colour to images at different times $t=0$ (red), $t=870$ (green), $t=1770$ (blue). Stationary FAs appear as white. Scale bar: $20\mu\text{m}$.

Supplementary Note I: Generation of expression constructs

Generation of the VinTS expression construct

Restriction sites were added to mTFP1 (5'XhoI/3'ApaI) and venusA206K cDNAs (5'NdeI/3'NotI) by polymerase chain reaction (PCR), and PCR products were inserted into pBluescript SK(-) (Stratagene, 212205) in which the multi-cloning site had been modified (5'XhoI-ApaI-NdeI-NotI3'). Oligonucleotides with ApaI and NdeI-compatible overhangs encoding a 40 aa flagelliform sequence (GPGGA₈) were annealed and inserted between mTFP1 and venusA206K (named: pSK-TSMod).

Next, chicken vinculin cDNA was amplified by PCR, Kozak-ATG, stop codon and restriction sites (5'HindIII/3'EcoRI) were added, and a Sall/NotI restriction site (5'-GTCGACGTCTATGCGGCCGCG-3') was generated after the codon for aa 883. This modified cDNA was inserted into pBluescript SK(-) in which Sall- and NotI-restriction sites had been deleted (pSK-vinculin-linker). TSMod cDNA (digested with XhoI/NotI) was then introduced into Sall/NotI-digested pSK-vinculin-linker (XhoI and Sall overhangs are compatible). This VinTS cDNA was inserted into the pcDNA3.1 expression vector (Invitrogen, V795-20) using HindIII/EcoRI restriction sites (pcDNA3.1 VinTS).

Generation of control constructs

The VinTL expression construct was generated by PCR using VinTS cDNA as a template. A stop codon was inserted after the venusA206K cDNA followed by a NotI restriction site. The PCR product was inserted into pcDNA3.1 using HindIII/NotI (pcDNA3.1 VinTL).

The TSMOD expression construct was generated by PCR using VinTL as a template. An EcoRI restriction site was generated in front of the mTFP1 sequence. This cDNA was inserted into pcDNA3.1 via EcoRI/NotI.

To generate the controls for intermolecular FRET (VinTi, VinVi) restriction sites were added to mTFP1 or venusA206K cDNA (5'Xho/3'Not) by PCR. PCR products were then inserted into SalI/NotI-digested pSK-vinculin-linker. cDNAs were inserted into pcDNA3.1 using HindIII/EcoRI.

To generate the mTFP1-venusA206K conformation sensor, the stop codon after vinculin in pSK-vinculin-linker was removed and mTFP1 was inserted into the vinculin cDNA using XhoI/NotI restriction sites. This vinculin-mTFP1 DNA was inserted into pcDNA3.1 via HindIII/EcoRI. VenusA206K with 5'EcoRI/3'XbaI restriction sites and stop codon was added after the vinculin-mTFP1 cDNA using EcoRI/XbaI.

To generate the vinculin-venus expression construct, Kozak-ATG and HindIII/EcoRI restriction sites were added to chicken vinculin cDNA by PCR, and the stop codon was removed. This cDNA was inserted into pcDNA3.1 via HindIII/EcoRI. VenusA206K cDNA with EcoRI/XbaI restriction sites and stop codon was introduced after the vinculin cDNA using EcoRI/XbaI.

Supplementary Note II: Detailed explanation of spectrofluorimetry, FRET analysis, FA segmentation, FA tracking, FRAP analysis, and FA stability measurements

Spectrofluorimetry

Hypotonic cell lysates were prepared from HEK293 cells as described²¹. Spectrofluorimetric analyses were performed with a Fluoromax-3 spectrofluorometer (Horiba Jobin Yvon). Excitation wavelengths were 458 nm (mTFP1) and 505 nm (venusA206K). Spectra were traced from 460 to 600 nm (increment: 0.5 nm, integration time: 0.1 s, slit width: 3 nm). FRET efficiencies were calculated using the acceptor ratio method³². Donor bleed-through was removed by fitting the emission spectrum of mTFP1 to the emission spectrum of the FRET construct over the range of 475-500 nm and subtracting the two spectra. The FRET efficiency was calculated by

$$E = \frac{\varepsilon_A(\lambda_{A,ex})}{\varepsilon_D(\lambda_{D,ex})} \left(\frac{I_{D,ex}(\lambda_{A,em})}{I_{A,ex}(\lambda_{A,em})} - \frac{\varepsilon_A(\lambda_{D,ex})}{\varepsilon_A(\lambda_{D,ex})} \right)$$

where ε_D and ε_A are the extinction coefficient for the donor and acceptor, λ represents wavelength for the excitation or emission of the donor and acceptor ($\lambda_{D,ex} = 462$ nm, $\lambda_{A,ex} = 505$ nm, $\lambda_{A,em} = 525$ nm), $I_{D,ex}(\lambda_{A,em})$ is the intensity of the bleed-through corrected construct spectrum at $\lambda_{A,em}$ when excited by $\lambda_{D,ex}$ light and $I_{A,ex}(\lambda_{A,em})$ is the intensity of construct emission spectra at $\lambda_{A,em}$ when excited by $\lambda_{A,ex}$.

Intensity-based FRET analysis

FRET analysis was performed with non-linear spectral bleed-through corrections²⁷. First, the pixel intensities of overexposed pixels were set to zero and images were background-subtracted using the average of 5 blank fields. Pixel intensities below a user-defined threshold, typically 5-10 % of the maximum intensity, were also set to zero.

Additionally the alignment of each set of FRET images was checked by shifting the images relative to each other and determining the maximum correlation coefficient. Almost all images were found to be optimally aligned without shifting.

Spectral bleed-through coefficients were determined using images of cells expressing either mTFP1 or venusA206K taken in the donor, acceptor and FRET channels. Typically 10 images were taken in each channel for a given transfection. To determine the donor bleed-through (dbt), the FRET image was divided by the mTFP1 image of cells transfected with mTFP1. These data were binned by the intensity of the mTFP1 image, averaged in each bin, interpolated with a cubic spline and the interpolation was smoothed with a boxcar average to create a non-linear function representing dbt as a function of intensity. Acceptor bleed-through (abt) was determined in the analogous way. Donor and acceptor cross-talks (donor fluorescence in the acceptor channel and *vice versa*) were found to be negligible and hence ignored. Background and spectral bleed-throughs were determined for each experiment.

To correct for spectral bleed-through in experimental data, pixel-by-pixel FRET corrections were performed according to the equation:

$$cFRET = FRET - dbt(I_D)I_D - abt(I_A)I_A$$

cFRET: corrected FRET image, I_D : donor image intensity, I_A : acceptor image intensity.

To normalize for variations in intensity, the *cFRET* values were divided by I_A and reported as the FRET Index.

FA segmentation

FAs were segmented using a version of the previously described water algorithm, adapted for 8-point connectivity²⁸. This enabled unique identification of individual FAs (Supplementary Fig.6). In experiments probing subcellular variations (Fig.3d, e and Fig.4a, b), these identifications were used to average the image values in individual FAs. This type of local averaging has the advantage of avoiding edges effects common to most types of filtering. Briefly, the venusA206K image was smoothed with a boxcar average, subtracted from the original image, and pixels below a user defined threshold were set to zero (Supplementary Fig.6). Remaining pixels were then sorted by brightness to form a descending list. Isolation of individual FAs was accomplished with the following set of rules while going through the list:

Case 1: If the selected pixel has no neighbouring pixels assigned to a FA, assign the pixel to a new FA.

Case 2: If the selected pixel has neighbouring pixels assigned to a single FA, assign the pixel to that FA.

Case 3: If the selected pixel has neighbouring pixels assigned to multiple FAs, merge the connected FAs to one new FA if the size of at least one of the connected FAs is less than a critical size for merger. If mergers do not occur, assign the pixel to the brightest neighbouring FA.

Typical parameters were found to be 25 pixels for the length scale of the box filter and 9-12 pixels for a minimum merger size. Setting a minimum area of 3-5 pixels removed falsely identified FAs due to intensity fluctuation in the cytoplasmic vinculin signal.

By looping over the pixels (ij) in a given FA mask (M) in either the donor, acceptor or FRET index image, various attributes of the FA, including area (A), centre of mass (i_c, j_c), and average intensity (I), can be calculated with the following formulae:

$$A = \sum_{ij|M=k} 1$$

$$i_c = \frac{\sum_{ij|M=k} I_{ij} i}{T}, j_c = \frac{\sum_{ij|M=k} I_{ij} j}{T}$$

where $T = \sum_{ij|M=k} I_{ij}$ and $I = \frac{T}{A}$

FA tracking

For tracking of individual FAs, the centres of mass determined for an entire movie were used in combination with previously described³⁰ and publicly available (<http://www.physics.emory.edu/~weeks/idl/>) particle tracking software. The data structure was altered so that the size, acceptor intensity, and FRET index of individual FAs could also be tracked through time. FAs that merged, split or were subject to high velocity movements were excluded from the analysis. FA Size Index was defined as the size of the FA in pixels multiplied by the average brightness of the FA. For comparison of multiple FAs this quantity was normalized to its maximum for a given trajectory. FAs that increased normalized size index from under 40 % to the maximum observed size were considered assembling, and FAs that shrank to less than 40 % of the maximum size were considered disassembling. Identification of a relatively small number of successfully tracked assembling or disassembling FAs (5-20 per cell) was conducted by manual examination of the trajectories. Trajectories were typically generated from particles that were identified in at least 9 consecutive frames. A maximum displacement for particles between frames was set between 5 and 7 pixels. Histograms of particle

displacement were checked to ensure displacements were smaller than this cut-off to prevent artificial trajectory truncation.

FRET metrics and normalizations

The standard metric for FRET analysis is FRET efficiency, the percentage of photons that undergo FRET. FRET efficiency is an instrument-independent measure and directly related to the separation distance of the fluorophores described by the Förster equation. FLIM, single molecule and spectroscopy measurements are reported in this form. In intensity-based microscopy measurements FRET is typically reported as FRET index and can take many forms³³. Here, it is the intensity in the FRET channel, corrected for spectral bleed-through, divided by the intensity in the acceptor channel. This metric is dependent on experimental settings and not easily related to the exact distance between the fluorophores.

For some measurements normalized version of these metrics were used. Specifically, to allow direct comparisons between two different FRET constructs, VinCS and VinTS (Supplementary Fig.3e), data were normalized to untreated controls. For cell migration analysis (Fig.3d-g) the relative differences between protruding and retracting areas in a single cell were to be analyzed. To account for cell-to-cell variation in the overall FRET, the FRET index of specific regions of the cell (protruding or retracting) was normalized by the average FRET index of the entire cell. Measurements of the FRET efficiency of TSMoD, VinTS and VinTL in solution (Fig.2b) were slightly higher (25-30 %) than FRET efficiencies determined by FLIM (22-25 %) probably due to differences in temperature, pH or salt concentration. As FLIM measurements in living cells were considered to be the more relevant measurement, the spectroscopy data were normalized to prevent confusion.

FRAP analysis

Six images were acquired before entire, single FAs were bleached. Cells were then imaged in the venusA206K channel every 5 s for 5 min. User-defined polygons were used to outline a background region outside the cells, the initial positions of at least two unbleached FAs and at least one bleached FA. Next, the FA polygons were refined with the water algorithm (see FA segmentation). To account for small FA movements of 2-20 pixels typical in these experiments³⁴, the original outline of the FAs was moved. To enable an automated analysis, a rough estimation of the FA was determined using a dilated version of polygon from the previous frame followed by refinement with the water algorithm. For the bleached FA, the position of the polygon was held constant while the intensity of the FA was under a user-defined threshold, typically 60 % of the initial intensity. FAs that merged, split, grew, shrank or moved drastically during the course of the experiment were not analyzed. Without these modifications, analysis of stationary polygons yielded downward sloping recovery curves at long times instead of asymptotic recovery.

To calculate the percentage of recovery, background was first subtracted from each FA. Then, to account for bleaching or focus fluctuations, the mean intensity of the background-subtracted bleached FA was divided by the average intensities of background-subtracted unbleached FAs from the same cells. Furthermore, to normalize the starting intensity and full recovery value to one, the curves were divided by the average value of the normalized curve in the pre-bleach pictures. This procedure is described in the following equations

$$\text{Normalized Recovery} = \frac{1}{N} \frac{\overline{I_{blch}(t)} - \overline{I_{bkg}(t)}}{\overline{I_{con}(t)} - \overline{I_{bkg}(t)}}$$

where $\overline{I(t)}$ represents the time varying, average fluorescence intensity. Different types of FAs are denoted as blch (bleached), bkg (background) and con (control). The normalization factor N is defined by

$$N = \sum_{i=0}^{npb} \frac{\overline{I_{blch}(t)} - \overline{I_{bkg}(t)}}{\overline{I_{con}(t)} - \overline{I_{bkg}(t)}}$$

where npb is the number of pre-bleach images that were taken. This recovery curve was then fit to a single exponential recovery equation²².

$$\text{Normalized Recovery} = R_f - (R_f - R_o)e^{-kt}$$

where R_f is the final recovery, R_o is the initial recovery, and k is recovery rate. The half-life of the recovery can be determined by $\tau_{1/2} = \ln 2/k$.

FA stability measurements

To measure FA stability, we adapted a previous technique²⁹. Intensities of individual FAs from the first frame of a time-lapse movie were compared to the same area in each consecutive frame to create decay curves. Masks of FAs were generated with the water algorithm from the initial frame of a time-lapse sequence. The total intensity of each mask was calculated through time until becoming equal to the background. These individual decay curves were averaged and normalized by their initial value. The faster the intensity decreases, the less stable the FA.

Supplementary Note III: Single molecule FRET-force measurements and tension sensor calibration.Fluorescence-force spectroscopy

A protocol for assembling samples for the fluorescence-force experiment was described previously². Briefly, a solution of 50 pM TSMoDCy construct was immobilized on a coverslip coated with polyethyleneglycol (mPEG-SC, Laysan Bio), which eliminated non-specific surface adsorption of proteins and reduced surface interactions with DNA and microspheres³⁵. The immobilization was mediated by biotin-Neutravidin binding between the biotinylated force sensor, Neutravidin (Pierce), and biotinylated polymer (Bio-PEG-SC, Laysan Bio). Next, anti-digoxigenin-coated 1 μm polystyrene microspheres (Polysciences) were added so that one microsphere could attach to the free end of each tethered molecule. Protein G-coated polystyrene microspheres (1.0 μm , Polysciences) were cross-linked to sheep anti-digoxigenin (Roche Applied Science) as described². For imaging, the buffer was: 10 mM Tris (pH 7.5), 1x PBS, 0.5 % (wt/vol) D-glucose (Sigma), 165 U/ml glucose oxidase (Sigma), 2170 U/ml catalase (Roche), 3 mM Trolox (Sigma), and 0.1 % (vol/vol) Tween 20 (Sigma).

Single molecule fluorescence-force experiments were performed at $22 \pm 1^\circ\text{C}$. The overall design of the apparatus has been described². Once a tethered microsphere was trapped, the sample was moved in two orthogonal directions with the piezo-stage to roughly determine the tethered position of the peptide construct. The piezo-stage was then moved back and forth between a starting position (typically 13.5 μm or 14 μm separation between the tethered point and the trap centre) to an end position (16.8-16.9 μm) at a constant speed of 455 nm s^{-1} for several cycles. The confocal excitation beam was programmed to follow the motion of the tethered force sensor molecule so that the

donor (Cy3) and acceptor (Cy5) fluorescence intensities were recorded with 44 ms time resolution as a function of applied force.

Single-molecule TIR spectroscopy

Wide-field prism-type total internal reflection (TIR) spectroscopy described previously³⁵ was used to determine the zero force FRET value of the Cy3/Cy5 sensor in the same imaging buffer as used in fluorescence-force spectroscopy. A single-molecule FRET histogram was generated by averaging for 300 ms. Background, cross-talk and gamma corrections were considered for calculating the FRET efficiency³⁵.

Calibration of VinTS

To apply the FRET vs. force calibration obtained for TSMoDCy to VinTS differences in geometry between the experiments as well as the different fluorophores must be accounted for. Because estimates of fluorophore and linker size are often difficult to determine with high accuracy, an approximation was utilized to relate TSMoDCy to TSMoD. The zero-force FRET efficiency of the Cy3-Cy5 based construct is ~50 % while FRET efficiency of TSMoD was ~23.5 %. Both constructs have Förster distances of ~6.0 nm. Therefore, adding 1.3 nm to the observed extension in the TSMoDCy makes the zero-force FRET efficiencies match. We further assume that this relationship is relatively constant throughout the stretching of VinTS and TSMoDCy.

To obtain the calibration curve we first calculated the inter-fluorophore distance R for TSMoDCy by inverting the Förster equation and utilizing the FRET efficiency of TSMoDCy at a given force. Then, $(R+1.3 \text{ nm})$ was inserted into the Förster equation as the inter-fluorophore distance to calculate the corresponding FRET efficiency of VinTS. The resulting FRET efficiency vs. force calibration curve for VinTS is shown in

Supplementary Fig.4b. For stable numerical conversion data were fit to a fourth order polynomial. FRET efficiencies were calculated from FLIM lifetimes (Fig.2c, d) and converted to apparent forces using this relationship (Supplementary Fig.4d, e). Based on this calibration, we estimated that the typical force on vinculin in FAs of living cells is about 2.5 pN.

Assessment of assumptions for calibration

The most critical assumption in this calibration is that measurements on TSMoD can readily be applied to VinTS. It is possible that the incorporation of TSMoD into vinculin or the application of force across VinTS could change the relative orientation of the fluorophores or inhibit their mobility. These effects would change FRET independent of separation distance. We find this scenario very unlikely for two reasons. First, FRET efficiency was not different in spectroscopic FRET measurements for TSMoD, VinTL or VinTS suggesting that incorporation into vinculin does not change the behaviour of TSMoD at zero force (Fig.2b). During force application, the variability of the FRET data in the single molecule stays relatively constant suggesting suppression of fluorophores mobility does not occur (Fig.2i).

Limitations of the tension sensor method

A problem inherent to any biosensor is that its insertion might interfere with the properties of the host protein, or the host protein might interfere with the function of the biosensor. Therefore, a careful evaluation is essential. We have shown that effects of this type are likely to be small for VinTS. VinV and VinTS are produced as stable proteins (Supplementary Fig.2a), they show normal localization to FAs (Supplementary Fig.1), have very similar FRAP rates (Fig.1g) and are both activated by actin and IpaA (Supplementary Fig.3e). We also showed that the FRET efficiency of TSMoD is not

altered by its insertion into vinculin (Fig.2b) and that inter-molecular FRET is negligible (Supplementary Fig.3c). Thus, in the context of our experiments and conclusions, potential limitations are small if not negligible. Whether absolute forces across vinculin are altered by insertion of TSMoD can not be directly checked. However, bulk estimates from traction force microscopy experiments or atomic force microscopy data can be used to evaluate the obtained results^{14,16}. While it is likely that TSMoD will be useful for other proteins analogous control experiments assessing the effects of TSMoD insertion on the module itself and the protein of interest will be essential for any newly generated tension sensor.

Supplementary References

- ³¹ Vicente-Manzanares, M. et al. Regulation of protrusion, adhesion dynamics, and polarity by myosins IIA and IIB in migrating cells. *J Cell Biol* 176, 573-580 (2007).
- ³² Majumdar, Z. K., Hickerson, R., Noller, H. F., and Clegg, R. M. Measurements of internal distance changes of the 30S ribosome using FRET with multiple donor-acceptor pairs: quantitative spectroscopic methods. *J Mol Biol* 351, 1123-1145 (2005).
- ³³ Jares-Erijman, E. A. and Jovin, T. M. FRET imaging. *Nat Biotechnol* 21, 1387-1395 (2003).
- ³⁴ Wehrle-Haller, B. Analysis of integrin dynamics by fluorescence recovery after photobleaching. *Methods Mol Biol* 370, 173-202 (2007).
- ³⁵ Roy, R., Hohng, S., and Ha, T. A practical guide to single-molecule FRET. *Nat Methods* 5, 507-516 (2008).